The Steady Linear Response of a Spherical Atmosphere to Thermal and Orographic Forcing[1]

BRIAN J. HOSKINS AND DAVID J. KAROLY[2]

U.K. Universities' Atmospheric Modelling Group and Department of Meteorology, University of Reading, RG6 2AU England

(Manuscript received 21 November 1980, in final form 23 February 1981)

ABSTRACT

Motivated by some results from barotropic models, a linearized steady-state five-layer baroclinic model is used to study the response of a spherical atmosphere to thermal and orographic forcing. At low levels the significant perturbations are confined to the neighborhood of the source and for midlatitude thermal forcing these perturbations are crucially dependent on the vertical distribution of the source. In the upper troposphere the sources generate wavetrains which are very similar to those given by barotropic models. For a low-latitude source, long wavelengths propagate strongly polewards as well as eastwards. Shorter wavelengths are trapped equatorward of the poleward flank of the jet, resulting in a split of the wavetrains at this latitude. Using reasonable dissipation magnitudes, the easiest way to produce an appreciable response in middle and high latitudes is by subtropical forcing. These results suggest an explanation for the shapes of patterns described in observational studies.

The theory for waves propagating in a slowly varying medium is applied to Rossby waves propagating in a barotropic atmosphere. The slow variation of the medium is associated with the sphericity of the domain and the latitudinal structure of the zonal wind. Rays along which wave activity propagates, the speeds of propagation, and the amplitudes and phases along these rays are determined for a constant angular velocity basic flow as well as a more realistic jet flow. They agree well with the observational and numerical model results and give a simple interpretation of them.

1. Introduction

The papers of Charney and Eliassen (1949) and Smagorinsky (1953) gave the first detailed account of the steady, linear response of an atmosphere to large scale orographic and thermal forcing. In these studies the sphericity of the earth was modeled using the β-plane approximation, thus allowing the possibility of Rossby wave motion. In the following years there have been numerous papers published on the effects of the two forcings. Derome and Wiin-Nielsen (1971) used a β-plane quasi-geostrophic model and Egger (1976a,b; 1977) a hemispheric two-level primitive equation model. General circulation models have also been used to try and isolate the role of mountains (Manabe and Terpstra, 1974; Kasahara *et al.*, 1973) and anomalous thermal sources (Rowntree, 1972, 1976; Chervin *et al.*, 1980, and refs.).

In an attempt to cast more light upon the behavior on the sphere of Rossby waves due to large scale sources and sinks, the propagation of energy and vorticity as described by the linearized, barotropic vorticity equation was examined in Hoskins *et al.* (1977). In Grose and Hoskins (1979) a barotropic model was used to study the steady, linear Rossby wave pattern on zonal flows induced by various simple mountains. It was found that there was a tendency to produce a split wavetrain downstream of a mountain range. For a Northern Hemisphere winter 300 mb zonal flow, the train poleward of 40° was composed of lower zonal wavenumbers than that equatorward of this latitude, and about 80° downstream of the mountain there was a tendency for a "blocked" region with a region of anticyclonic vorticity located poleward of a cyclonic vorticity region.

It is of interest to attempt the modeling of thermal sources using barotropic models. For midlatitudes this is scarcely possible because of the baroclinic nature of the local response to thermal forcing. However, for tropical regions one may argue (following Bjerknes, 1966) that an anomalously warm ocean may lead to extra convective heating in the atmosphere. This will be balanced by extra upward motion and hence divergence and forcing of anticyclonic vorticity at upper levels. Thus the simplest model of a tropical thermal anomaly is to force anticyclonic vorticity in a tropical region in a non-divergent barotropic model which is linearized about a zonal flow.

Many experiments have been performed with such a model, but little sensitivity of the solutions is found. We shall present one typical case here. The zonal flow is a climatological Northern Hemisphere 300 mb winter flow, the negative vorticity source is in an elliptical region between the equator and 30°N and

[1] Contribution No. 7, Joint Institute for the Study of the Atmosphere and Ocean, University of Washington/NOAA.

[2] Present affiliation: Australian Numerical Meteorology Research Centre, Melbourne, Australia.

0022-4928/81/061179-18$08.50

between 30°W and 30°E. To make the total vorticity source zero, a uniform positive vorticity source is placed elsewhere at these latitudes. As was done in Grose and Hoskins (1979), a linear wave drag with an e-folding time of 14.7 days and a scale selective ∇^4 smoothing are included. The model is time dependent, hemispheric and uses a spectral representation with triangular truncation at total wavenumber 42. The forcing is switched on at $t = 0$. The answers obtained are clearly linearly proportional to the magnitude of the forcing. However, to be definite, we take the maximum upper level divergence to be 4×10^{-6} s^{-1}. This is approximately the value of the convergence that would be expected to give an extra 10 mm of rain per day.

Ater ten days the solution changes little with time and 30-day averages are not far from steady-state solutions. The 30-day average perturbation vorticity field is shown in Fig. 1. There is a negative response as expected over the source but the interesting feature is the propagation north and east from the source. The corresponding height field, as obtained from the linear balance equation, shows a 6 dam high slightly west of the forcing, a low of 17 dam centered on 35°N, 10°E, a similar high near 60°N, 40°E and a low at 70°N, 110°E of 11 dam. These features are set up by approximately 2, 4, 6 and 10 days, respectively. There is clearly a measure of agreement with the description of Bjerknes (1966), in particular the strengthening of the subtropical jet and a trough to the north. The height field deviations are similar in magnitude to the largest anomalies found in monthly mean charts.

The barotropic calculations of wavetrains described in Grose and Hoskins (1979) and here are interesting because of both the nature of the solutions and their suggestive similarity with observed teleconnection patterns, as will be discussed below. However, the linearized barotropic model is clearly a great simplification of atmospheric behavior. As a step closer to reality, in this paper we look for the patterns predicted by a hemispherical baroclinic model. The model is linearized and steady state; the presence of baroclinic instability precludes a simple time-marching approach. It uses five equally spaced layers in the vertical, which are almost certainly not sufficient to represent the longest waves in certain circumstances, this being a subject of current study.

Details of the model and methods of solution are given in Section 2. In Sections 3 and 4 the responses to thermal and orographic forcing are exhibited. Away from the forcing regions the results show an equivalent barotropic structure with largest amplitudes in the upper troposphere; the 300 mb level patterns are very similar to those predicted using barotropic theory.

These results are consistent with those from recent observational studies. Blackmon *et al.* (1979) have used 15 years of NMC data to study the geographical variations in the vertical structure of geopotential height fluctuations. They particularly noted the barotropic nature of fluctuations on time scales of a week to a season over the eastern oceans, compared with their baroclinic nature over the continents. This is in agreement with the barotropic nature of the model results if these long time scale transients are forced by changes in the flow over orography and in the thermal input from the continental and western boundary current regions. Wallace and Gutzler (1981) have used the NMC monthly mean winter data to make an objective search for teleconnections in the geopotential height field. They identified these teleconnections by correlating the 500 mb geopotential (or sea-level pressure) at every point with every other point and seeking extrema in the correlation coefficients. They identified five dominant patterns and produced composite charts for these patterns. Again, the patterns were essentially equivalent barotropic, but hemispheric teleconnections were more evident at the 500 mb level. Further work by Horel and Wallace (1981) has shown that warm episodes in equatorial sea-surface temperature in the Pacific tend to be accompanied by below-normal 700 mb height in the North Pacific, above-normal heights over western Canada, and below normal heights over the southeastern United States. All the teleconnection patterns are very reminiscent of the Rossby wavetrains in the model results.

In Section 5 the wavetrains in the models and atmosphere are interpreted using the theory for waves propagating in a slowly varying medium. The waves considered are stationary, barotropic Rossby waves and the variation of the medium is due to the sphericity of the earth as well as the latitudinal structure of the zonal flow. The patterns, time-scales and amplitudes deduced from the theory agree with those given by the numerical model.

2. Model details and method of solution

The basic numerical model used for this study is the primitive equation, σ-coordinate model described by Hoskins and Simmons (1975). It uses the spectral-transform technique in the horizontal and second-order finite differences in the vertical and has been thoroughly tested and used in many studies of baroclinic instability. In a linearized calculation, the solution for each zonal wavenumber m is independent and may be determined separately. On the hemisphere, using a rhomboidal truncation, at level j the vorticity variable ξ which is an odd function about the equator is represented by

$$\xi = [\xi^{j,m}_{m+1} P^m_{m+1}(\mu) + \xi^{j,m}_{m+3} P^m_{m+3}(\mu) + \cdots + \xi^{j,m}_{m+J} P^m_{m+J}(\mu)] e^{im\lambda},$$

where μ = sin(latitude), λ = longitude and P_n^m are the associated Legendre functions and it has been assumed that J is odd. Variables even about the equator, e.g., divergence D, are represented by

$$D = [D_m^{j,m}P_m^m(\mu) + D_{m+2}^{j,m}P_{m+2}^m(\mu) + \cdots + D_{m+J-1}^{j,m}P_{m+J-1}^m(\mu)]e^{im\lambda}.$$

The atmospheric state in wavenumber m may be described by the vector

$$\mathbf{X} = (\xi, i\mathbf{D}, \mathbf{T}, \ln\mathbf{p}_*), \tag{2.1}$$

where

$$\xi = (r_{m+1}\xi_{m+1}^{1,m}, \ldots, r_{m+J}\xi_{m+J}^{1,m}, r_{m+1}\xi_{m+1}^{2,m} \cdots, r_{m+J}\xi_{m+J}^{NL,m}), \tag{2.2}$$

$$\mathbb{D} = (r_m D_m^{1,m} \cdots, r_{m+J-1}D_{m+J-1}^{1,m}, \ldots, r_{m+J}D_{m+J-1}^{NL,m}), \tag{2.3}$$

$$\mathbb{T} = (T_m^{1,m}, \ldots, T_{m+J-1}^{1,m}, \ldots, T_{m+J-1}^{NL,m}), \tag{2.4}$$

$$\ln\mathbf{p}_* = (\ln p_{*m}^m, \ldots, \ln p_{*m+J-1}^m), \tag{2.5}$$

T is the temperature, p_* the surface pressure, $r_n = [n(n+1)]^{-1/2}$ and NL the number of model levels. It is easily shown that the linearized primitive equations with no source or sink terms may be written

$$\dot{\mathbf{X}} = i\mathsf{A}\mathbf{X}, \tag{2.6}$$

where A is a real square matrix of side $(3 \times \mathrm{NL} + 1) \times (J+1)/2$. The r_n factors are included in (2.2) and (2.3) to make more of the elements of A of order 1. Given a working time-dependent model, the matrix A may be simply determined a column at a time by performing a sequence of single time-steps using as initial conditions the zonal flow plus unity in one component of X. For example, (2.6) shows that initial conditions with $X_k = \delta_{k,l}$ give

$$\dot{\mathbf{X}}_j = i\mathsf{A}_{jl}, \tag{2.7}$$

and so the lth column of the matrix A is given by $-i\dot{\mathbf{X}}$.

For the steady problem with forcing F and linear dissipation $D\mathbf{X}$, Eq. (2.6) is modified to become

$$0 = i\mathsf{A}\mathbf{X} + D\mathbf{X} + \mathbf{F}.$$

The steady response to the forcing F is thus

$$\mathbf{X} = i(\mathsf{A} - iD)^{-1}\mathbf{F}. \tag{2.8}$$

After determination of the matrix A for a particular zonal flow, the solution as given by (2.8) may be calculated using routine matrix inversion or Gaussian elimination algorithms.

Every solution obtained is checked by substitution into an independent version of the spectral primitive equation model, the forcing and dissipation also being included.

The dissipation on ξ is taken to be of the form

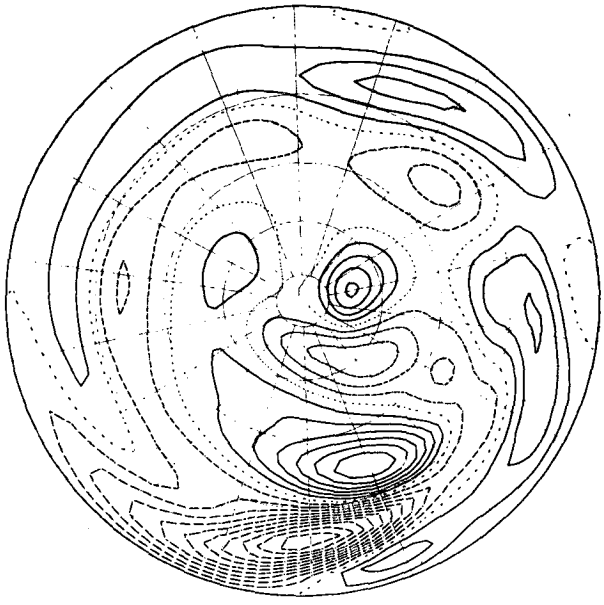

FIG. 1. 30-day average perturbation vorticity field for a negative vorticity source in the region 0–30°N, 30°W–30°E switched on at $t = 0$ using a hemispheric barotropic model linearized about a Northern Hemisphere 300 mb winter zonal flow. The map projection is polar stereographic with lines of latitude and longitude drawn every 20°. Negative contours are dashed, the zero contour dotted and positive contours continuous. With magnitudes specified in the text, the contour interval is 0.05Ω.

$$-\lambda_U(\sigma)\xi - K\nabla_h^4\xi. \tag{2.9}$$

That on D is of similar form. The temperature dissipation is

$$-\lambda_T(\sigma)T' - K\nabla_h^4T'. \tag{2.10}$$

The simple λ term is used to represent the effects of the boundary layer, damping due to radiation and the influence of transient eddies. In (2.10),

$$T' = T - \ln p_* \frac{dT(\sigma)}{d\ln\sigma}$$

is a measure of the temperature perturbation on a pressure surface as opposed to a σ surface. Thus the dissipation matrix D is not diagonal. As in Grose and Hoskins (1979) the biharmonic horizontal diffusion is included so that critical lines at which the zonal flow velocity is zero are treated in a linear, dissipative manner. The value of K used in most experiments is again 2.338×10^{16} m^4 s^{-1}.

For the results described in this paper five equally spaced vertical levels are used. Thus ξ, D and T are represented at $p/p_* = 0.1, 0.3, 0.5, 0.7$ and 0.9. The spectral truncation is set at $J = 25$ so that each variable, on the hemisphere, for each zonal wavenumber and level, is described by 13 complex coefficients. The vector X has 208 components and the matrices are 208×208. For many cases 26 zonal wavenumbers are considered but the variance in the high

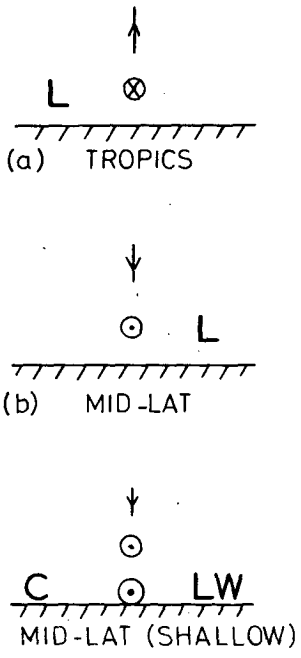

FIG. 2. Longitude-height sections showing the differing responses to thermal forcing in (a) tropics, (b) midlatitudes, and (c) mid-latitudes for shallow forcing. The arrow depicts vertical motion, circled crosses and dots motion into and out of the section, respectively, L the pressure trough, and C and W cold and warm air, respectively.

wavenumbers is very small and sometimes this number is reduced to six.

The zonal flow which is prescribed for most solutions is a Northern Hemisphere winter flow. The velocities are taken from Oort and Rasmusson (1971)[3] and modified to ensure symmetry about the equator. The temperatures and surface pressure are obtained from a balancing procedure described in Hoskins and Simmons (1975).

3. Thermal forcing

a. Introduction

In this section we shall exhibit the response to various thermal sources. In particular, the change of the response with the latitude and vertical distribution of the forcing will be discussed. As an aid to understanding the results it is worth constructing some simple arguments based on linearized, inviscid, β-plane vorticity (ξ') and potential temperature (θ') equations including a heating term Q. Using standard notation, these may be written

$$\bar{u}\xi_x' + \beta v' = fw_z', \tag{3.1}$$

$$\bar{u}\theta_x' + v'\bar{\theta}_y + w'\bar{\theta}_z = (\theta_0/g)Q. \tag{3.2a}$$

Using the thermal wind relations, the latter may be written

$$f\bar{u}v_z' - f\bar{u}_z v' + w'N^2 = Q. \tag{3.2b}$$

We consider first the balance of terms in the thermodynamic equation (3.2b): if zonal advection is dominant, $v' \sim QH_Q/f\bar{u}$, and if meridional advection is dominant, $v' \sim QH_u/f\bar{u}$. Here $H_Q = Q/Q_z$ and $H_u = \bar{u}/\bar{u}_z$ are the height scales of the heat source and the zonal velocity. However, if vertical advection is dominant, which is only possible away from the surface of the earth, $w' \sim Q/N^2$. In this case the stretching term in the vorticity equation (3.1) is $fw_z' \sim fQ/(N^2H_Q)$. For large horizontal scales, $k \ll k_s = (\beta/\bar{u})^{1/2}$, the β term must balance the stretching and

$$v' \sim fQ/(\beta N^2 H_Q).$$

Assuming that the mechanism requiring the smallest v' will dominate, it is seen that heating at and near the surface of the earth is balanced by horizontal temperature advection with the zonal or meridional component dominating according to whether H_u is greater or less than H_Q. Defining H to be the minimum of H_u and H_Q and $\gamma = f^2\bar{u}/(\beta N^2 H_Q H)$ then, away from the surface of the earth, heating is balanced by horizontal advection if $\gamma \gg 1$ and by vertical advection if $\gamma \ll 1$. For a situation with $H_u \lesssim H_Q \sim$ scale height, γ is the important parameter in baroclinic instability discussed by Held (1978) and others.

In the tropics, γ is small provided H_Q is greater than 1 km. Any heating at or near the surface would produce extremely large values of v'. A heat source ($Q > 0$) away from the surface is balanced by upward motion [$w' > 0$ in (3.2)] as sketched in Fig. 2a. This implies low-level creation of vorticity [$\partial w/\partial z > 0$ in (3.1)]. For waves with $k \ll k_s$, (wavelengths much longer than 3000 km, e.g.) this stretching must be balanced by the β term with poleward meridional motion. Thus it follows that the surface trough must be to the west of the thermal source.

The midlatitude situation, as discussed by Smagorinsky, is in complete contrast. There γ is generally large and heating at any level is balanced by horizontal advection of temperature. If H_Q is much larger than H_u (~1–2 km at low levels) a heat source is balanced by advection of cooler air from polar regions i.e., $v' < 0$ in the Northern Hemisphere. Thus the trough must be to the east of the source. For waves with $k \ll k_s$ (which for low levels in midlatitudes implies wavelengths much larger than 3000 km e.g.) the creation of vorticity associated with the β term in the vorticity equation must be balanced by vortex shrinking ($\partial w'/\partial z < 0$). In the absence of Ekman pumping this would imply descent in the region of the heat source. This situation is sketched in Fig. 2b. For shallow sources with $H_Q \sim H_u$, the low-level heating is partially balanced by zonal advection with the temperature gradient in the direction of flow. As shown in Fig. 2c, this is consistent

[3] Oort, A. H., and E. R. Rasmusson, 1971: Atmospheric circulation statistics. NOAA Prof. Paper No. 5. [U.S. Govt. Printing Office, Stock No. 0317-0045, c 55.25:5.]

with a maximum advection of cooler air from the pole at low levels and, again, a trough to the east.

b. A subtropical forcing

We now consider the response predicted by the baroclinic model described in section 2 for an isolated thermal forcing in the subtropics. The horizontal distribution of the source is that of a cosine squared in an ellipse on the tangent plane at 15°N of eccentricity 4 and minor axis 16° of latitude. Thus there is negligible forcing outside the latitudinal band 7–23°. At each latitude the zonal average is removed and so outside the longitudinal band ± 33° there is zonally uniform cooling. The heating region is indicated below in Fig. 3c. The vertical heating profile for this case is proportional to $\sin\pi\sigma$, having a maximum at 500 mb. Since the calculations are linear, the amplitude of the forcing is required only to give ideas on the magnitudes of responses. For this purpose we take the maximum vertically averaged heating rate (before removing the zonal average) to be 2.5 K day^{-1} which is approximately the latent heat release given by an extra 10 mm precipitation per day. As well as the standard biharmonic diffusion we include linear damping on the velocity and temperature waves at the lowest model level with e-folding time of 5 days, this being mainly a representation of boundary layer processes. At the higher model levels there is damping on the temperature wave only with e-folding time 10 days. This represents the dissipative effects of the transient eddies (Lau, 1979) and radiative processes. The zonal flow about which the model is linearized is that observed in the Northern Hemisphere winter.

In agreement with the description in Fig. 2a, the vertical velocity field induced by the heating is upward in the region of the source and has a three-dimensional distribution almost identical with that of the source. The maximum ascent at 900 mb is 22 mb day^{-1} and at 500 mb is 67 mb day^{-1}. The height field structure in the vicinity of the source is shown in Fig. 3a which is a longitude-height section at 18.1°N. The vertical structure is somewhat similar to that of the first internal mode. Gill (1980) assumed this structure and used the equatorial β-plane approximation in his study of the response of the tropical atmosphere to thermal forcing. In agreement with Gill's results, about 15° west of the source, there is a perturbation pressure maximum at upper levels and minimum at lower levels. The corresponding surface pressure perturbation minimum is −2.6 mb. The 900 mb poleward wind is a maximum of 2.2 m s^{-1} at the source and the 900 mb temperature a maximum of 2.2 K. The overall picture in the vicinity of the source is consistent with that given in Fig. 2a.

The low-level perturbations are mostly confined to the region of the source, but this is not true in the upper troposphere. Fig. 3b shows the 300 mb

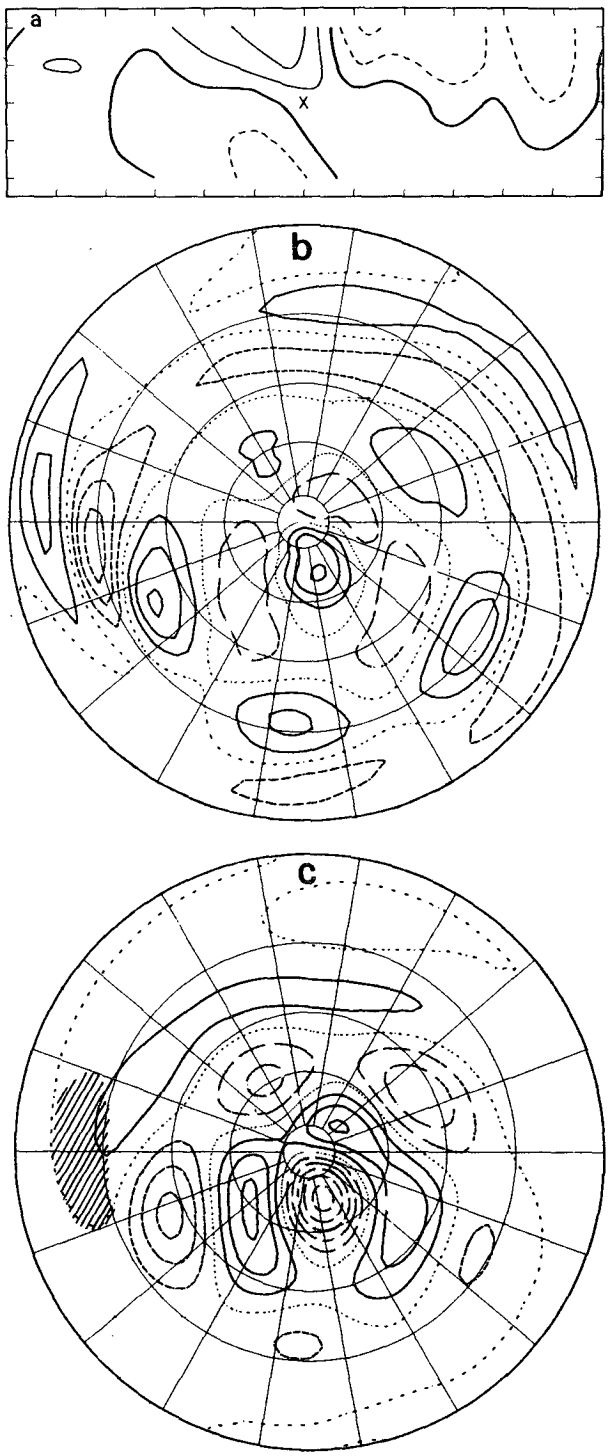

FIG. 3. Steady state, linear solution of a five-layer baroclinic model for a deep elliptical heat source at 15° perturbing the Northern Hemisphere winter zonal flow. Shown are (a) height field in a longitude-height section at 18.1°N (contour interval 1 dam), (b) 300 mb vorticity perturbation (contour interval 0.05Ω), and (c) 300 mb height field perturbation (contour interval 2 dam). The contour convention is as in Fig. 1 except that the zero contours in (a) are thick continuous lines. The center of the source is indicated by a cross in (a) and the region of heating larger than 0.5 K day^{-1} by hatching in (c). Tick marks in (a) are at 100, 300, 500, 700 and 900 mb in the vertical and every 30° of longitude.

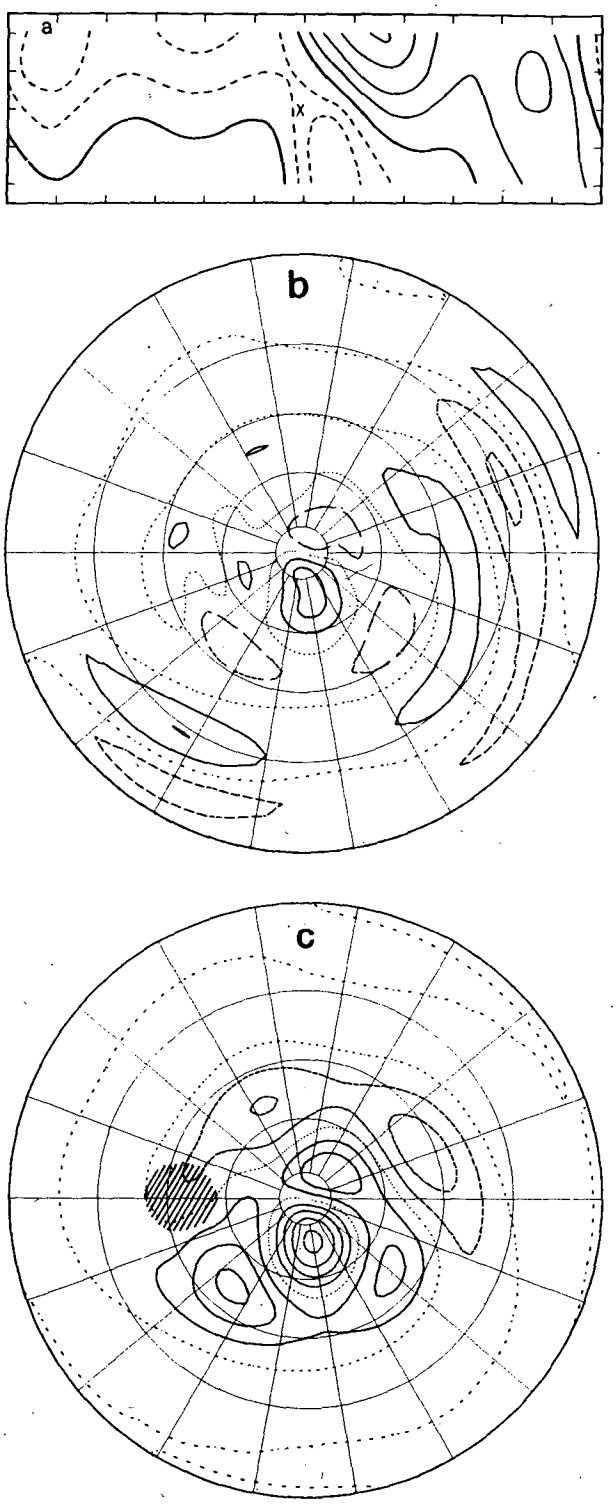

FIG. 4. Solution for a deep circular heat source at 45° using the NH winter flow. Shown are (a) height field in a longitude-height section at 46.0°N, (b) 300 mb vorticity perturbation, and (c) 300 mb height field perturbation. Contours as in Fig. 3, except that the contour interval in (a) is now 2 dam.

vorticity perturbation. The pattern is remarkably similar to that given in Fig. 1 for the barotropic model. Although the solution is steady, following the barotropic integrations, it is helpful to think of a train of waves being set up poleward and eastward of the source. About 60° downstream, at latitude 35°, there are signs of a split with the lower zonal wavenumbers continuing polewards to produce a maximum near 70° latitude and 110° downstream while the higher wavenumbers turn equatorwards. The polar wavetrain appears to proceed on towards the equator on the opposite side of the hemisphere. Typical upper-level vorticity amplitudes are $0.15-0.20\Omega$. The corresponding 300 mb height field perturbation, given in Fig. 3c, emphasizes the poleward portion of the pattern with a maximum high and low of 6.5 dam and 11 dam, respectively.

c. Some mid-latitude forcings

We now consider an identical problem except that the thermal source is centered at 45° and its horizontal distribution (illustrated in Fig. 4c) is circular, having the same area as the ellipse used in the subtropical forcing. The height field perturbation in a longitude–height section at latitude 46.0° is given in Fig. 4a. As suggested by the analysis in Section 3a, the balance of terms is clearly very different. The surface low pressure of 6.5 mb is attained 18° to the east of the source and the upper-level pressure maximum around 60° east. The heating at 900 mb is balanced by a equatorward wind of 3.7 m s^{-1}. At middle levels the height scale H_u of the zonal wind is ~8 km. Thus the balance is by zonal advection with the warmest air to the east of the source. 180° downstream from the source there are large amplitudes at upper levels, but these are better discussed in the context of 300 mb maps.

The 300 mb vorticity perturbation is shown in Fig. 4b and is again of hemispheric extent. There are positive values in the region of the source but the wavetrains appear to originate some 30° downstream with longer wavelengths propagating equatorwards as well as polewards. The corresponding height field perturbation (Fig. 4c) has a middle and high latitude distribution rather similar to that produced by the subtropical source. The magnitudes are, if anything, slightly smaller. The upper tropospheric pattern is very similar in shape and magnitude if the 45° source has an elliptical distribution. Thus, given that the source amplitude we have chosen is probably quite reasonable for the tropics but rather large for midlatitudes, we come to the conclusion that for the dissipation used herein it is easier to force a height field anomaly of a given amplitude in middle and high latitudes with a heating

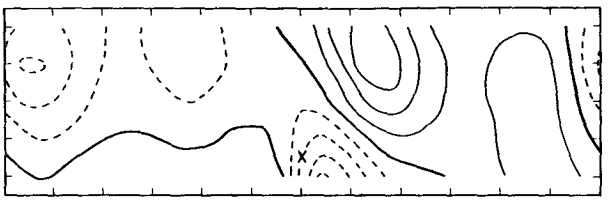

FIG. 5. Height field in a longitude-height section at 46.0°N for a shallow circular heat source at 45° with the NH winter flow. The contour interval is 2 dam.

anomaly in the subtropics than it is with one in middle and high latitudes.

It is an interesting feature of this solution that the 900 mb temperature perturbation is negative in the region of the heating, reaching −2.7 K approximately 7° east of the source maximum. This is however very dependent on the vertical distribution of the forcing. A solution has also been obtained for a source at 45° having the same horizontal distribution and vertically averaged heating but with a vertical distribution $\sigma^4 \sin\pi\sigma$, giving heating rates of 0.0, 0.2, 1.7, 5.2 and 5.4 K per day at $\sigma = 0.1, 0.3, 0.5, 0.7$ and 0.9, respectively. The longitude-height section at 46.0° for this source is given in Fig. 5. The low-level trough is intensified, the surface pressure minimum now being 12.6 mb. The temperature perturbation is +2.1 K at the source maximum rising to +5.2 K 18° downstream. The upper tropospheric fields are not very dependent on the vertical distribution and are very similar to those shown in Fig. 4.

The sensitivity of the low-level temperature to the vertical distribution of the midlatitude source is consistent with Figs. 2b and 2c, and the thermal wind relation $f\xi_z' \propto \theta'_{xx} + \theta'_{yy} \sim -\theta$, i.e.

deep heating →

positive vorticity increasing with height ↔

negative temperature perturbation,

shallow heating →

positive vorticity decreasing with height ↔

positive temperature perturbation.

It might be thought that the shallow heating case is clearly the relevant one away from the tropics. However, the upward eddy flux of heat by transient eddies of many scales could give the effective heating a deep distribution on some occasions.

The vertical velocity field in both deep and shallow midlatitude heating experiments exhibits weak ascent ahead of the heating and descent behind, the extrema being less than 10 mb day^{-1}.

d. Some other cases

Numerous other solutions have been obtained for different source latitudes, wave damping, biharmonic dissipation and basic zonal flows. Table 1 summarizes some of the information for different source distributions. For a forcing centered on the equator, not only is the vorticity generation by basic stretching small (f small) but also the source is completely within the region of easterly zonal winds at all heights. In accord with numerous other studies the response outside the latitude of forcing is small. As the source is moved polewards, the

TABLE 1. Experiments with different heat source distributions. The sources are denoted by the latitude of their maxima, their eccentricity, latitudinal extent and vertical distribution with D representing the $\sin\pi\sigma$ deep source and S the $\sigma^4 \sin\pi\sigma$ shallow source. The values given for surface pressure trough, 500 mb vertical velocity and 900 mb meridional wind and temperature are the extrema in the vicinity of the source. Where no value is given, there is no definite extremum in that vicinity. The pressure trough position is its longitude from the source. The last number is a subjective measure of the strength of the polar wavetrain at 300 mb, taking that for the deep 15° source as the unit.

Latitude (deg)	Eccentricity	Latitudinal extent (deg)	Vertical distribution	P_{*min} (mb)	P_{*min} position (deg)	ω_{500} (mb day^{-1})	v_{900} (m s^{-1})	T_{900} (K)	Polar wave
0	4	16	D	0.5	0	−45	−0.3	0.8	0.1
10	4	16	D	1.3	−11	−50	1.3	1.1	0.5
15	4	16	D	2.6	−14	−67	2.2	2.1	1.0
20	4	16	D	5.3	−13	−79		3.9	1.0
30	4	16	D	9.1	+25		−3.9	−5.2	0.8
45	4	16	D	7.0	+25		−2.7	−2.3	0.8
45	1	32	D	6.5	+21		−3.7	−2.9	0.8
45	1	32	S	12.6	+14		−5.8	5.2	0.7
45	1	64	S	18.7	+11		−5.8	10.6	1.8
60	1	32	S	22.1	+15		−8.2	8.4	0.9

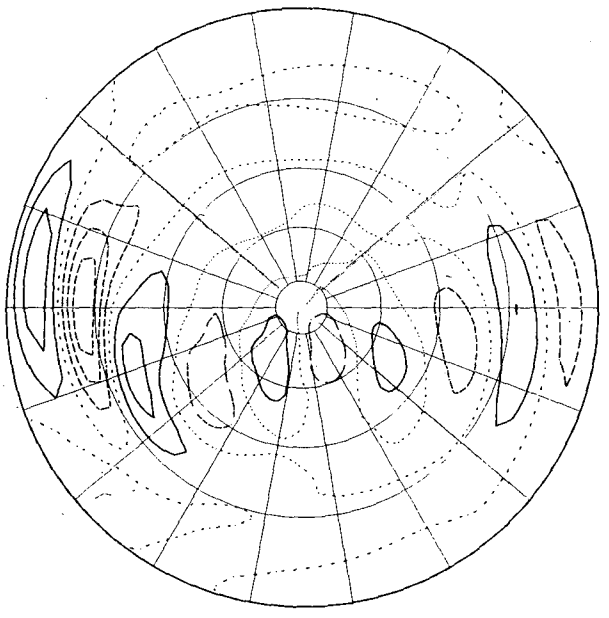

FIG. 6. 300 mb vorticity perturbation for a heat source at 15° when the basic flow is 0.7 times that used for Fig. 3. Contours as in Fig. 3b.

phase of the poleward wavetrain changes but its trajectory is very similar. Between 20° and 30° there is a change from the balance of the heating by vertical motion to the balance by horizontal advection. A source of double the radius of the previous one at 45° produces a polar wavetrain larger by a factor of 2 consistent with the increase in the long-wave components in the forcing. Finally we note that a shallow source gives a much larger low-level response if it is placed at 60° rather than at 45° because of the smaller meridional temperature gradient and hence larger compensating meridional wind required at the higher latitude.

The various damping experiments will not be described in detail here as the dominant effect is on fluxes of heat and potential vorticity and not on the wavetrain pattern which is the subject of this paper. The phases and amplitudes in this pattern are remarkably insensitive to the temperature damping. Increasing the velocity damping at levels 1–4 from zero to a value equivalent to a 10-day e-folding time gives a negligible change in the wavetrain pattern for a 15° deep source though the amplitudes are reduced by 40% locally up to a factor of 4 at the polar maximum.

For the same 15° source the biharmonic dissipation has been increased by a factor of 5 and decreased by factors of 2 and 5. The increase by 5 and decrease by 2 do not modify the wavetrain pattern. They produce only small changes in the amplitude near the source rising to a decrease of a factor of 3 and increase of a factor of 1.4 in the respective cases. However, the decrease of K by 5 results in a different pattern, this value probably being insufficient for the zero wind line to act as an absorber. In this case the equatorial wall would act as a spurious reflector.

The additional zonal flows that have been used are in three different categories. Those in the first category are obtained by multiplying the Northern Hemisphere winter zonal velocities by a certain factor. This factor has been varied from 0.7–1.4 in steps of 0.1. The 300 mb vorticity perturbation for a deep elliptical source at 15° in the weakest flow (0.7) is given in Fig. 6. It shows a simple poleward and eastward wavetrain whose trajectory is very similar to that for the basic flow (Fig. 3b). However the wavelength along the trajectory is rather shorter. As the zonal flow is increased, one gradually obtains more structure in the wavetrain after it has reached polar latitudes and more evidence of shorter waves turning equatorward near latitude 35°. However, when the factor is increased to 1.2 there is a dramatic change with zonal wavenumber 3 up by a factor of more than 5. This resonance will be discussed below. For even stronger flows, the response tends to be dominated by wavenumber 1 though the amplitude is not indicative of resonance.

The second type of zonal flow is obtained by adding a constant angular velocity equivalent to 3 m s^{-1} at the equator to the basic flow at all levels. The deep elliptical source at 15° gives a very similar response although, compared with Fig. 3c, the 300 mb high near 60°N is ~20° to the east and the 800 mb low is rather weaker and 35° to the east. The shallow 45° source gives a response about ⅔ of that without the superrotation, though otherwise similar. The smaller amplitude is due to more compensation by the larger zonal advection ($\bar{u}\partial\theta'/\partial x$). The third type of zonal flow has velocities at each level with latitudinal profile like $\sin^2[\pi \sin(\text{latitude})]$, having a maximum at 30°. Again the same qualitative pictures are obtained.

4. Orographic forcing

a. Introduction

Again it is worth considering simple arguments on the response to orographic forcing before considering linearized solutions to the primitive equations on the sphere. β-plane channel barotropic theory says that fluid columns are squashed on the upslope and stretched on the downslope, thus generating anticyclonic and cyclonic vorticity, respectively. For long wavelengths ($k < k_s$) the β term in the vorticity equation (3.1) is dominant and there is a cyclone over the ridge. Conversely, for medium and short wavelengths ($k > k_s$) the zonal vorticity advection dominates and there is an anticyclone over the ridge. At $k = k_s$ there is resonance

and the amplitude is limited only by the amount of dissipation present. The presence of dissipation moves the anticyclone towards the upslope forcing region for k both less than or greater than k_s, so that the solutions look as in Fig. 7a, b.

However, as suggested by the analysis of Dickinson (1978),[4] the situation is very different for the baroclinic case. In β-plane quasi-geostrophic theory, the topography (height h^*) enters only through application of the thermodynamic equation (3.2b) at the boundary with Q replaced by $-\bar{u}h_x^* N^2$. There is adiabatic cooling on the upslope and warming on the downslope. Since the ratio of the first to the second term in (3.2) is $(v'/v_z'):(\bar{u}/\bar{u}_z)$, for vertical scales much larger than 1–2 km, the upslope cooling must be balanced predominantly by the motion of warm air poleward ($v' > 0$) and the downslope warming counteracted by equatorward motion of cold air ($v' < 0$). Thus the anticyclone always tends to sit approximately over the mountain. For long wavelengths ($k < k_s$) the waves must be propagating in the vertical, slope westward with height and have the warmest air ahead of the trough. So that zonal advection may aid in counteracting the apparent heat source and sink the anticyclone shifts a little (typically less than 20°) westward of the mountain as shown in Fig. 7c. For short wavelengths ($k > k_s$) the waves are trapped (Fig. 7d). The wavelength ($k = k_s$) represents a simple transition between the two.

Barotropic theories have generally been applied to the middle and upper troposphere for which k_s corresponds to a wavelength of order 7 000 km so that for all except the very longest waves the relevant barotropic case is the shortwave one ($k > k_s$) shown in Fig. 7b. For baroclinic theories the relevant k_s is the lower tropospheric value which corresponds to a wavelength of about 3 000 km. Thus the most relevant case for medium and long wavelengths is the longwave one ($k < k_s$) in Fig. 7c. As commented by Dickinson (loc. cit.) it is largely fortuitous that barotropic theory with damping and baroclinic theory give the same phases in the most relevant region in parameter space. However, it is possible that the wavetrain away from the source region is, at least qualitatively, well described by barotropic theory.

b. A circular mountain at 30°

As was done with the thermal forcing, we shall first discuss one particular solution. The zonal flow is again that for the Northern Hemisphere winter.

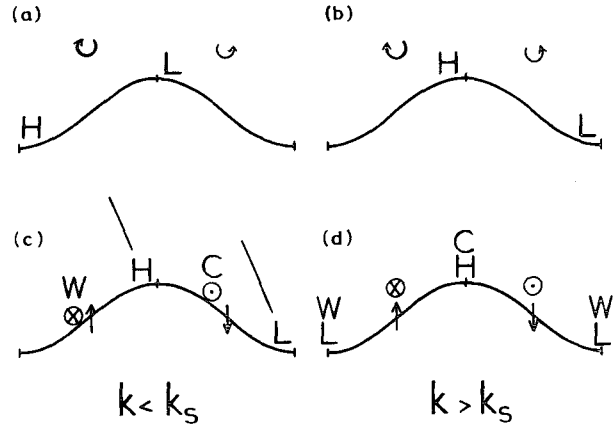

FIG. 7. Vertical sections showing the response to westerly flow over topography as described in the text. (a) and (b) are barotropic atmospheres with clockwise and counterclockwise arrows signifying the generation of anticyclonic and cyclonic vorticity, and H and L the pressure ridge and trough. (c) and (d) are baroclinic atmospheres with circled crosses and dots signifying poleward and equatorward flow, W and C the warmest and coldest air, H and L the mean sea-level pressure ridge and trough, and lines from them showing the vertical tilt of the pressure wave.

We include the standard biharmonic diffusion and a linear damping with e-folding times in days (10, ∞, ∞, ∞, 5) on velocity and (10, 10, 10, 10, 5) on temperature. The upper-level damping on velocity was included to compensate to some extent for the lack of loss of wave activity to the stratosphere. The mountain is taken to have a cosine-squared profile in a circle of diameter 45° of latitude centered at 30°N. For quantitative discussion the height of the mountain will be 2 km. Zonally averaged topography does not affect the linearized problem and when this is removed the 500 m contour is as shown below in Fig. 8d.

To emphasize the drawbacks of the linearized treatment of topography it should be noted that the low-level vertical velocity has a quadrupole pattern. The westerly winds poleward of 30° give the upslope region to the west of the mountain while the low-level easterly winds on the equatorward side give their upslope region to the east of the mountain. This implies very different low-level perturbation structures in the two regions as is apparent from the two vertical height-field sections shown in Fig. 8a, b. At latitude 40.5° there is a mean sea-level pressure maximum of 4.5 mb centered 3° west of the mountain top and a minimum of 3.1 mb ~ 33° to the east. There are negative 900 mb temperature perturbations over and to the east of the mountain (minimum −2.1 K) corresponding to a decrease of the ridge and increase of the trough with height. There are slight westward tilts with height and maximum amplitudes at 300 mb and 100 mb. This structure is consistent with the arguments given in

[4] Dickinson, R. E., 1978: On planetary waves. *The General Circulation: Theory, Modelling and Observations*. NCAR Summer 1978 Colloquium, NCAR/CQ–6+ 1978–ASP, 59–82.

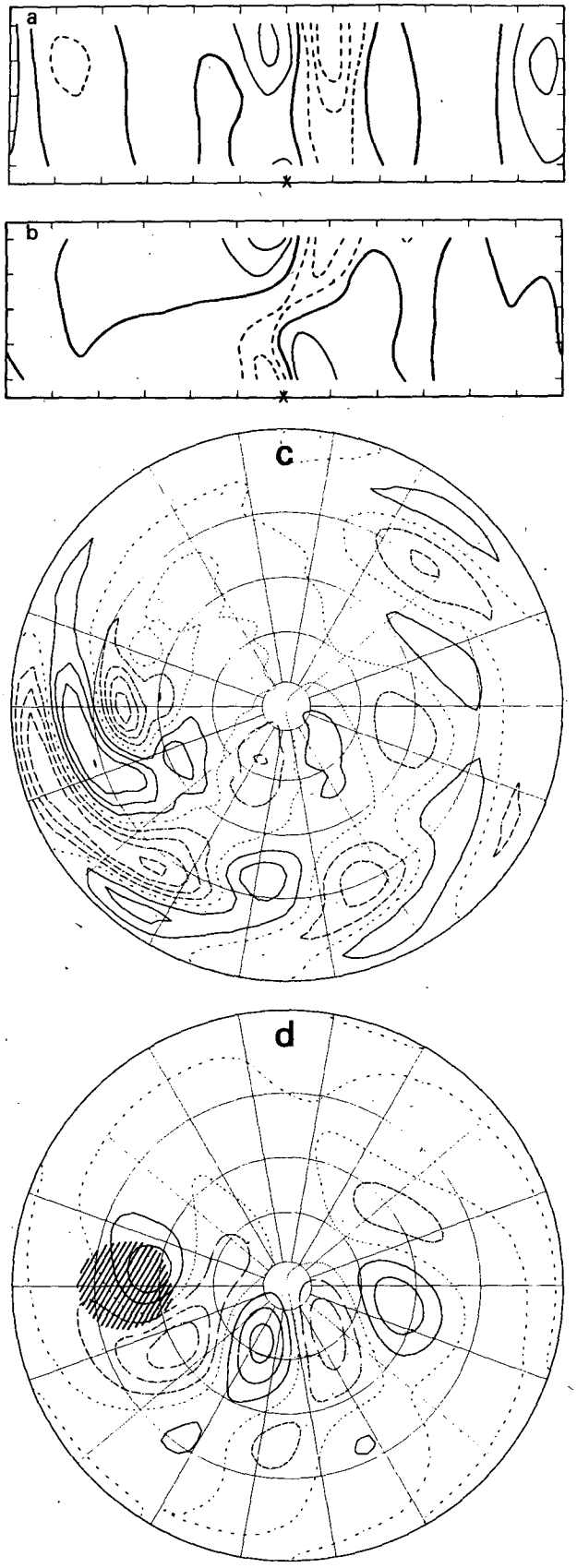

the previous section. They are also consistent with the low-level structure at latitude 23.7°. There the low-level wind is easterly and there is a mean sea-level pressure minimum of 7.1 mb centered 9° to the west of the mountain top and a maximum of 5.2 mb 18° to the east. Just above 900 mb the wind becomes westerly and the low-level response of opposite sign to that further north is replaced at upper levels by a pattern in phase with that for the north.

Again the interesting hemispheric patterns have maximum amplitudes in the middle and upper troposphere. The 300 mb vorticity and height field perturbations, given in Fig. 8c, d are very similar to those predicted by the barotropic model (Grose and Hoskins, 1979). In particular there is a low wavenumber polar wavetrain and a shorter wavelength subtropical train, with a split near latitude 40°. About 80° downstream of the mountain there are positive height field deviations poleward of negative deviations: an incipient blocking region. Upper tropospheric height perturbations are in the range 6–8 dam, quite similar to those given by 2.5 K day^{-1} thermal sources.

c. *Some other simple mountain cases*

It is arguable that a zonal wind representative of, say, the 950 mb level instead of that at 1000 mb should be used to evaluate the topographic ascent and descent in a linearized model. The stronger westerly winds at the higher level would imply more forcing in the westerlies and a transition to easterlies nearer the equator. As a measure of the possible effect of such a modification, the solution is obtained for the same problem but with the zonal flow everywhere increased by a constant angular velocity equivalent to 3 m s^{-1} at the equator. The surface transition to easterlies is moved equatorwards by ~5° to latitude 26°. The 300 mb vorticity perturbation (Fig. 9) shows some changes near the mountain equatorward of 35° but the downstream wavetrains differ only in their slightly greater wavelength.

A 30° mountain with horizontal dimensions reduced by $\sqrt{2}$ gives a similar pattern but the polar wavetrain is smaller by a factor of 4, consistent with the reduced amplitude in the longest wavelengths. If the original circular mountain is elongated meridionally conserving its area, the amplitudes of the long wavelengths in the mountain are reduced but this is compensated by increased amplitude in the region of large surface westerlies. If the circular

FIG. 8. Solution for a circular mountain at 30° with the NH winter flow. Shown are (a) height field in a section at 40.5°N, (b) height field in a section at 23.7°N, (c) 300 mb vorticity perturbation (d) 300 mb height field perturbation. The contours are as in Fig. 4. Shown also in (d) is the 500 m contour of the mountain.

mountain is moved to 60° there is a very similar polar wavetrain and an equatorward train also of long wavelength.

d. Earth orography

It is not the intention of this paper to see how closely linear models can simulate the observed stationary wave pattern. However, it is of interest to determine the response to perturbing the observed Northern Hemisphere winter zonally averaged zonal flow with a smoothed orography. The actual orography used was essentially the T21 version exhibited in Hoskins (1980) except that symmetry about the equator was imposed. The model 300 mb height field perturbation (Fig. 10) picks out the polar wavetrains from the Himalayas, the Rockies and, to a small extent, Greenland; to make this clear, solutions have been obtained for the three separately. The Himalayas generate half the ridge at 75°, almost all the extrema at 120°, 160° and 230° and positive and negative centers at 265° and 315°. The Rockies upstream ridge and downstream trough at 235° and 280° are not well in phase with the latter two and they combine to give the extrema at 250° and 292°. The Rockies generate a ridge at 320° which is reinforced by Greenland, the trough at 20° and half the ridge at 75°.

Compared with the observed 300 mb pattern the main difference is the shorter wavelength, particularly in the Pacific sector. This is consistent with the fact that the barotropic model gave a more realistic answer using the 300 mb flow than the 500 mb

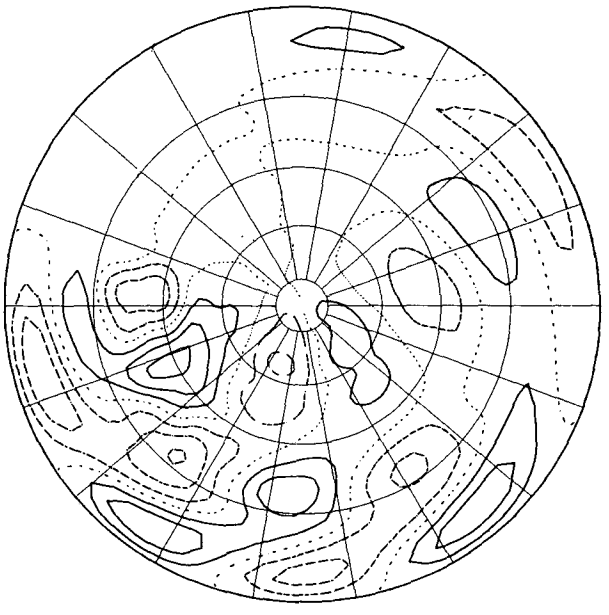

FIG. 9. 300 mb vorticity perturbation for a circular mountain at 30° with the NH winter flow augmented by a super-rotation. Contours as in Fig. 3.

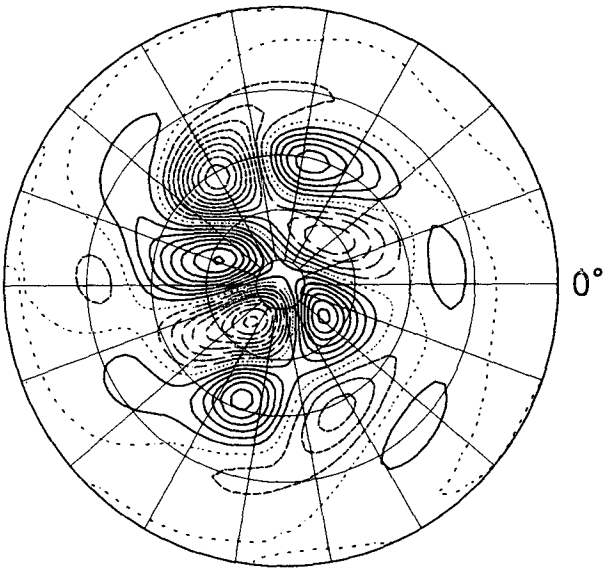

FIG. 10. 300 mb height field perturbation for the NH earth orography using the NH winter flow. Contours as in Fig. 3. The Greenwich Meridian is indicated.

flow. At least two possibilities occur. First, it is possible that linearized theory is not valid. In particular, the ambient flow in the Pacific sector is much stronger than the zonal average. For example, the climatological zonal wavenumber 1 implies that the average zonal wind in the latitude band 30–45°N is about 5 m s^{-1} larger in the sector 80–260°E than the zonal average. If the experiment is repeated with the zonal flow augmented by the 3 m s^{-1} angular velocity, a pattern much closer to the observed is obtained. Secondly, it is clear from Section 3 that we may expect thermal forcing to be important in the winter climatology. In particular, the low-level Aleutian and Atlantic lows are very probably thermally forced. In this connection, it is of interest to note that the two experiments mentioned give mean sea level pressure highs of 10.1 and 16.6 mb at 84°E, 40.5°N and 8.4 and 6.7 mb at 110°W, 40.5°N, suggesting that significant portions of the Siberian high and the high over the western United States may be associated directly with the response to orographic uplift.

5. Rossby wave rays

a. Introduction

Some of the most interesting points to come out of the above investigation are as follows:

(i) Away from the source region the wavetrains produced in the upper troposphere of the baroclinic model and in the barotropic models are qualitatively and even quantitatively very similar.

(ii) Long wavelengths (i.e., small zonal wavenumbers) propagate strongly polewards as well as

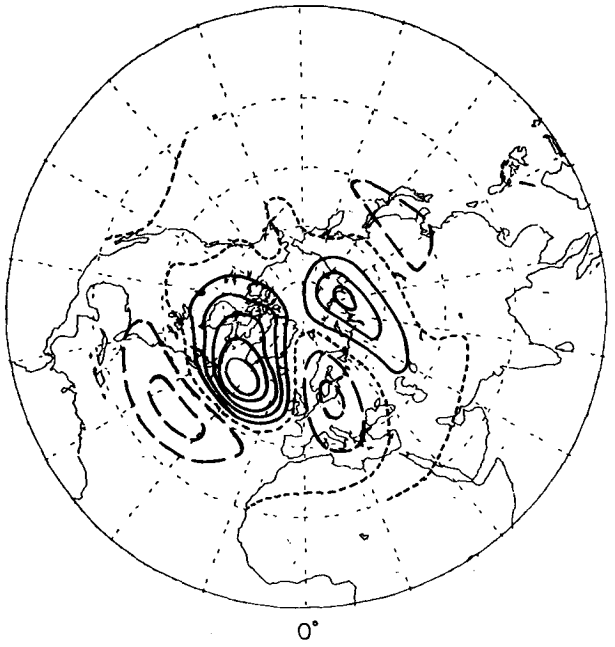

FIG. 11. The western Atlantic pattern at 500 mb found by Wallace and Gutzler (1980, adapted from their Fig. 21). Shown is the difference between the 10 months with the largest positive value of an index of the pattern and the 10 months with the largest negative values in a set of 45 winter months. The contour interval is 4 dam. Interpreting the contours as in Fig. 3, the picture may be taken as typical of the winter months with a large positive value of the index.

eastwards, resulting in a wavetrain path not very dissimilar from a great circle.

(iii) Shorter wavelengths appear to be trapped equatorward of the poleward flank of the jet (~40°), resulting in a split of the wavetrains at this latitude and a possible "blocking" region downstream where the long, poleward wavetrain and shorter, subtropical wavetrain are out of phase.

(iv) With the dissipation used here, the easiest way to produce a prescribed amplitude in middle and high latitudes is by subtropical forcing.

(v) The low-level temperature field for midlatitude thermal forcing is crucially dependent on the vertical distribution of the source.

Of these five points, the fifth has been explained above using the thermal wind relation. The first point is clarified somewhat when it is pointed out that the wavetrains in the baroclinic model have an equivalent barotropic structure, with their height or streamfunction perturbations having the same sign throughout the depth. Amplitudes are largest in the upper troposphere and almost everywhere there is an equivalent barotropic level between 500 and 200 mb.

(i) is also consistent with the barotropic nature of fluctuations over the eastern oceans as discussed by Blackmon *et al.* (1979) and of the teleconnections found by Wallace and Gutzler (1981). These teleconnection patterns are, indeed, very reminiscent of the wavetrains illustrated in this paper and suggest that this feature found in simple linearized, steady-state model is of importance in the earth's atmosphere. As an example, we give in Fig. 11 an adaptation of Wallace and Gutzler's map of the western Atlantic pattern; shown is the difference in 500 mb height between their ten months with the most positive and the ten months with the most negative values of an index of the pattern. This pattern was reproducible in an independent data set for 13 previous winters though some of the others were less clearly identifiable.

The GCM studies of Rowntree (1972, 1976a,b) have given indications of similar wavetrains and large middle and high latitude perturbations in response to subtropical forcing. Lau (personal communication) has found that the difference maps between GCM runs with and without mountains also display these patterns.

In the rest of Section 5 we apply kinematic wave theory and ideas from geometrical optics to a barotropic model in order to understand the existence of wavetrains and, in particular, points (ii) to (iv).

b. Barotropic Rossby waves in a slowly varying medium

We shall consider solutions of the linearized nondivergent barotropic vorticity equation on the sphere. It is convenient to use a Mercator projection of the sphere (e.g., Phillips, 1973):

$$x = a\lambda, \tag{5.1}$$

$$y = a \ln[(1 + \sin\phi)/\cos\phi]. \tag{5.2}$$

Then

$$\frac{1}{a\cos\phi}\frac{\partial}{\partial\lambda} = \frac{1}{\cos\phi}\frac{\partial}{\partial x}, \tag{5.3}$$

$$\frac{1}{a}\frac{\partial}{\partial\phi} = \frac{1}{\cos\phi}\frac{\partial}{\partial y}, \tag{5.4}$$

$$\nabla^2 = \frac{1}{\cos^2\phi}\left(\frac{\partial^2}{\partial x^2} + \frac{\partial^2}{\partial y^2}\right), \tag{5.5}$$

$$\cos\phi = \operatorname{sech} y/a, \tag{5.6}$$

$$\sin\phi = \tanh y/a. \tag{5.7}$$

The Mercator basic zonal velocity

$$\bar{u}_M = \bar{u}/\cos\phi \tag{5.8}$$

is proportional to the angular velocity. The equation for the horizontal streamfunction perturbation ψ, on multiplying by $\cos^2\phi$, takes the form

$$\left(\frac{\partial}{\partial t} + \bar{u}_M\frac{\partial}{\partial x}\right)\left(\frac{\partial^2\psi}{\partial x^2} + \frac{\partial^2\psi}{\partial y^2}\right) + \beta_M\frac{\partial\psi}{\partial x} = 0, \tag{5.9}$$

where

$$\beta_M = \frac{2\Omega}{a}\cos^2\phi - \frac{d}{dy}\frac{1}{\cos^2\phi}\frac{d}{dy}(\cos^2\phi\bar{u}_M) \quad (5.10)$$

is $\cos\phi$ times the meridional gradient of the absolute vorticity on the sphere.

The dispersion equation for plane wave solutions $\exp i(kx + ly - \omega t)$ of (5.9)

$$\omega = \bar{u}_M k - \frac{\beta_M k}{k^2 + l^2}. \quad (5.11)$$

As described by Whitham (1960), for example, the activity of almost-plane waves moves with the group velocity

$$\mathbf{c}_g = (u_g, v_g),$$

where

$$u_g = \frac{\partial\omega}{\partial k} = \frac{\omega}{k} + \frac{2\beta_M k^2}{(k^2 + l^2)^2}, \quad (5.12)$$

$$v_g = \frac{\partial\omega}{\partial l} = \frac{2\beta_M kl}{(k^2 + l^2)^2}. \quad (5.13)$$

Defining a ray to be everywhere in the direction of the local $\mathbf{c}_g$, energy propagates along a ray with speed equal to the group velocity. Since the dispersion equation (5.11) has no explicit dependence on x and t, kinematic wave theory gives that k and ω must be constant along a ray. The meridional wavenumber varies along the ray such that (5.11) is satisfied everywhere.

To describe stationary wave phenomena we consider the case $\omega = 0$. Then a ray is given by

$$\frac{dy}{dx} = \frac{v_g}{u_g} = \frac{l}{k}, \quad (5.14)$$

and along a ray k = constant and

$$k^2 + l^2 = K_s^2, \quad (5.15)$$

where the "stationary wavenumber" is

$$K_s = (\beta_M/\bar{u}_M)^{1/2}. \quad (5.16)$$

From (5.12) and (5.13), the magnitude of the group velocity is

$$c_g = 2\frac{k}{K_s}\bar{u}_M. \quad (5.17)$$

Thus on the Mercator projection or on the sphere, energy propagates along a ray at a speed double that of the component of the basic flow in the direction of the ray.

To obtain a more definite idea of amplitude and phase corresponding to a given zonal wavenumber and frequency we follow the ideas of WKBJ theory (e.g., Dingle, 1973) and look for a solution

$$\psi = P(y)\exp i(kx - \omega t). \quad (5.18)$$

Substitution in (5.9) gives

$$\frac{d^2P}{dy^2} + l^2P = 0, \quad (5.19)$$

where

$$l^2(y) = \frac{K_s^2}{1 - \omega/k\bar{u}_M} - k^2. \quad (5.20)$$

Assuming $P(y) = C\exp if(y)$, the usual WKBJ approximate solution is

$$f(y) = \int^y l(y)dy + \tfrac{1}{2}i\ln l(y), \quad (5.21)$$

this being valid provided

$$|dl^{-1}/dy| < 1, \quad (5.22)$$

i.e., provided the length scale l^{-1} is slowly varying. Thus the approximate form for ψ is

$$\psi = Cl^{-1/2}\exp\left[i\left(kx + \int^y ldy - \omega t\right)\right]. \quad (5.23)$$

To be definite, consider a wave of zero frequency propagating polewards and eastwards. Assuming K_s is a decreasing function of latitude, l decreases (5.15), the ray path becomes more zonally oriented (5.14) and the streamfunction amplitude increases (5.23). The latitude at which $K_s = k$ then provides a turning point for the ray. Near this latitude the WKBJ approximate solution (5.23) is not valid and it can be shown that the latitudinal behavior of the amplitude is that of an Airy function. Its wavelike structure can be matched onto the ray solution equatorward of the turning point. Poleward of this point it is evanescent. As the ray moves equatorwards the WKBJ solution is again valid. If there is a critical line $y = y_c$ at which $\bar{u} = 0$, then approaching y_c the ray tends to become meridional and the group velocity tends to zero. The WKBJ solution is not valid close to the critical line but a local analysis can be performed. In a linear, dissipative model the wave energy is absorbed, though the realism of this is frequently questioned (e.g., Tung, 1979).

The poleward increase in amplitude along a ray is important enough that it is worth considering an alternative derivation of the $l^{-1/2}$ factor in the streamfunction amplitude $\hat{\psi}$. Bretherton and Garrett (1969) introduced the concept of the conservation of wave action along rays. The wave action density is

$$A = \frac{E}{\omega - k\bar{u}_M},$$

where E is the wave energy density

$$\frac{1}{2}\left[\left(\frac{\partial\psi}{\partial x}\right)^2 + \left(\frac{\partial\psi}{\partial y}\right)^2\right].$$

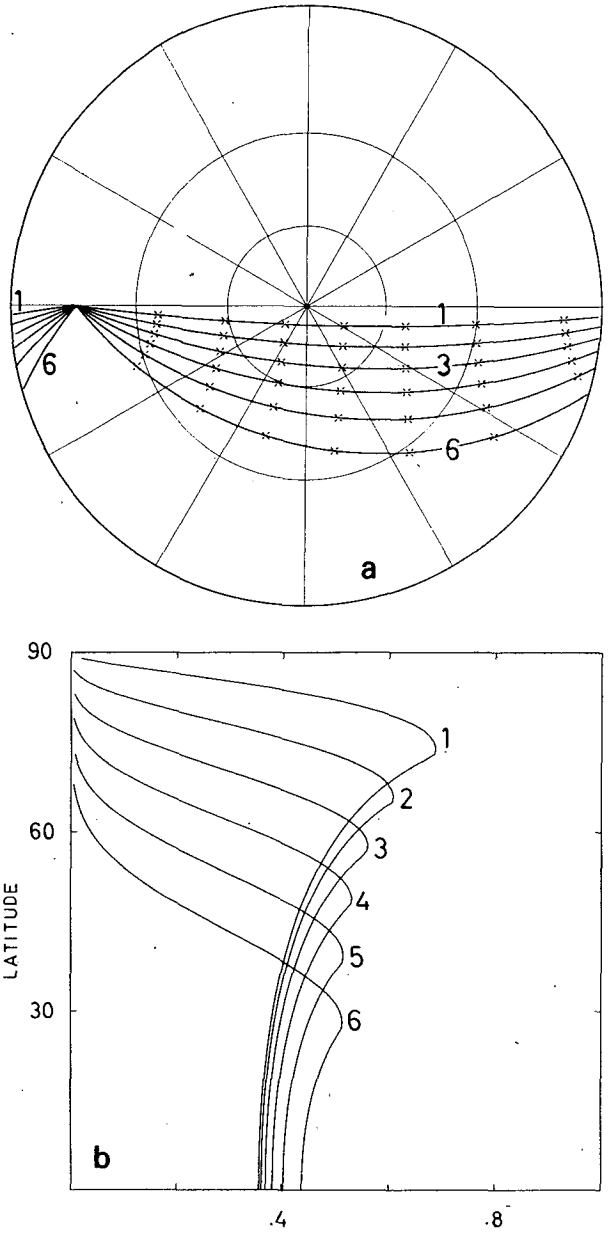

FIG. 12. (a) Rays and phases marked by a cross every 180° for a source at 15° in a super-rotation flow. If all wavelengths give a negative extremum at the source, the crosses mark the positions of successive positive and negative extrema. Lines of latitude and longitude are drawn every 30° and the zonal wavenumbers associated with the rays are indicated. (b) Amplitudes of the extrema on the rays for the different zonal wavenumbers, on the super-rotation flow shown as a function of latitude. The relative amplitudes of the different wavenumbers depend on the position and nature of the source.

For a medium dependent only on y, as discussed by Lighthill (1978) for example, $v_g A$ is constant along a ray. v_g is given by (5.13) which may be rewritten $2(k\bar{u}_M - \omega)l/(k^2 + l^2)$. E is $\frac{1}{2}(k^2 + l^2)\hat{\psi}^2$. Thus $l\hat{\psi}^2$ must be constant along a ray, again giving the $l^{-1/2}$ factor in the streamfunction amplitude. Viewed in this way, one may associate the increase in streamfunction amplitude as a wave propagates towards a turning point with the decrease in the poleward group velocity.

c. A constant angular velocity flow

In Section d, the above slowly varying wave theory will be applied to realistic zonal flows. However many of the results are little different from those obtained with a constant angular velocity flow: $\bar{u}_M = a\tilde{\omega}$. Thus we shall first produce the analytical results of this case.

From (5.10),

$$\beta_M = \frac{2\cos^2\phi}{a}(\Omega + \tilde{\omega}), \tag{5.24}$$

and the stationary wavenumber (5.16) is

$$K_s = (\epsilon a)^{-1}\cos\phi, \tag{5.25}$$

where $\epsilon^2 = \tilde{\omega}[2(\Omega + \tilde{\omega})]^{-1}$. From (5.14) and (5.15), the rays are given by

$$\frac{dy}{dx} = \left(\frac{K_s^2}{k^2} - 1\right)^{1/2}. \tag{5.26}$$

Substituting (5.25) into (5.26) and using $d\phi/d\lambda = \cos\phi(dy/dx)$, Eq. (5.26) may be integrated giving the ray equation

$$\tan\phi = \tan\alpha \sin(\lambda - \lambda_0), \tag{5.27}$$

where

$$\cos\alpha = \epsilon a k. \tag{5.28}$$

Eq. (5.27) is the equation for a great circle through $\lambda = \lambda_0$, $\phi = 0$ and reaching a latitude α given by (5.28) which from (5.25) is where $K_s = k$. The result that the rays for this case are great circles was given by the work of Longuet-Higgins (1964). From (5.25), the wavelength *on the sphere* at the turning point of every ray is ϵ times the planetary circumference. From (5.17) and (5.25), the speed of energy propagation in the great circle path on the sphere is $2\epsilon ak(a\tilde{\omega})$, i.e., a constant directly proportional to the zonal wavenumber. Thus the time taken for energy to propagate 90° in longitude from the equator to the turning point is $(2\epsilon ak)^{-1}$ times the time for the zonal flow to travel 90°.

For actual numbers, we refer to the constant angular velocity (super-rotation) flow used in Hoskins *et al.* (1977) and Grose and Hoskins (1979). The speed at the equator was ~15 m s^{-1}, $\tilde{\omega}/\Omega = 1/30.875$ and $\epsilon \sim 0.125$. Thus the wavenumber one great circle reaches up to 83° but, traveling at 3.8 m s^{-1}, the time taken for activity to propagate from the equator to this turning point is ~31 days. Wavenumber two, traveling twice as fast, reaches 76° in ~15.5 days. The fastest possible energy propagation time around the sphere is 15.5 days. The wavelength on the sphere at any turning point is ~5000 km. Actual rays along with the phases computed from the WKBJ solutions agree to remarkable accuracy with the solutions for super-rotation forcing problems shown in Fig. 7 of Hoskins *et al.* (1977) and Fig. 3 of

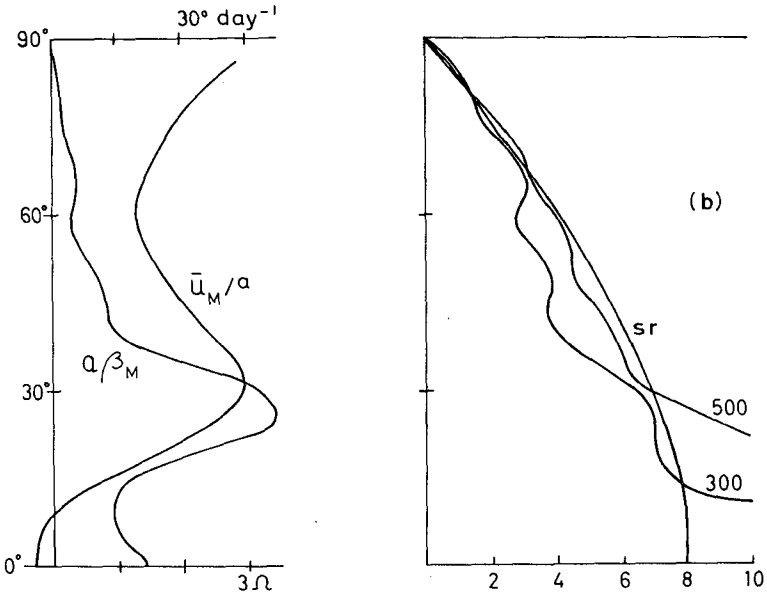

FIG. 13. (a) $\bar{u}_M/a$ (deg day^{-1}) and $a\beta_M$ for the 300 mb NH winter flow used in the model. (b) Stationary wavenumbers aK_s for the super-rotation flow, and the 500 and 300 mb NH winter flow.

Grose and Hoskins (1979). The former computation was a time-dependent one in which the downstream waves were set up consecutively and the integration was stopped at day 8, the train having reached almost 180° downstream of the source. The latter solution was a steady state for a model including a wave damping with e-folding time of 14.7 days. Consistent with the above numbers, the longest wavelengths had little amplitude near 180° and even the shortest waves were damped by the time that they had propagated back to the source. Thus with the value of dissipation used, or a larger one, resonance plays little part in the solution and the only sensitive aspect of the solution is the amplitude of the downstream wavetrain.

For comparison with later solutions, we show in Fig. 12 the rays and phases on a polar stereographic map for a source at 15° and the amplitudes predicted in the waves in the absence of dissipation. The relative amplitudes and indeed the presence of the different zonal wavenumbers depend on the latitude and shape of the forcing. The large gain in amplitude in the lowest wavenumbers as they propagate polewards must be balanced against the long time for this propagation and thus the probable large wave damping.

It is worth noting at this point that, for strict application of the wave theories, the zonal periodicity of the sphere should be dropped. Then the zonal wavenumber ak would be a continuous variable and the pictures shown for integer values should be taken as characteristic of zonal wavenumbers in a band centered on that value. The application of these ideas to the periodic sphere is valid only when propagation around the whole sphere is impossible due to damping (or absorption at a critical line) or to time limitation as in the cases discussed above, i.e., in cases without resonance.

d. More realistic flows

Plots of $\bar{u}_M$, β_M and K_s for the Northern Hemisphere winter 300 mb flow used in the five-level model solutions are given in Fig. 13. The main difference from the superrotation case is that β_M is large in the jet and small to the north, making K_s drop from a value of 7 in the jet to less than 4 at 45°. Thus, in agreement with point (iii) above, we may expect wavenumbers 4 and larger to be trapped by the northern flank of the jet while the longer wavelengths can propagate to 60°. Shown also in Fig. 13 is the stationary wave profile for the 500 mb flow. Taking the flow at this level allows wavenumber 4 to reach almost 60° as well.

There is some small-scale structure in the 300 mb K_s that makes the validity of the WKBJ solution dubious. Because of this, a slight smoothing is applied to the basic flow. The calculated wave amplitudes are shown in Fig. 14. In Fig. 15 are given the rays, energy propagation times and phases for a 15° source, and the rays and phases for 30° and 45° sources are illustrated in Fig. 16. The streamfunction amplitudes show an increase with latitude similar to that with the super-rotation. Again the possible effects of dissipation have to be noted, although with the stronger velocities the time-scales are shorter. As can be seen from Fig. 15a, wavenumber one propagates from 15° into the 60° latitude circle within 9 days. For wavenumber two, the time is only 5 days. The phases shown in Fig. 15b

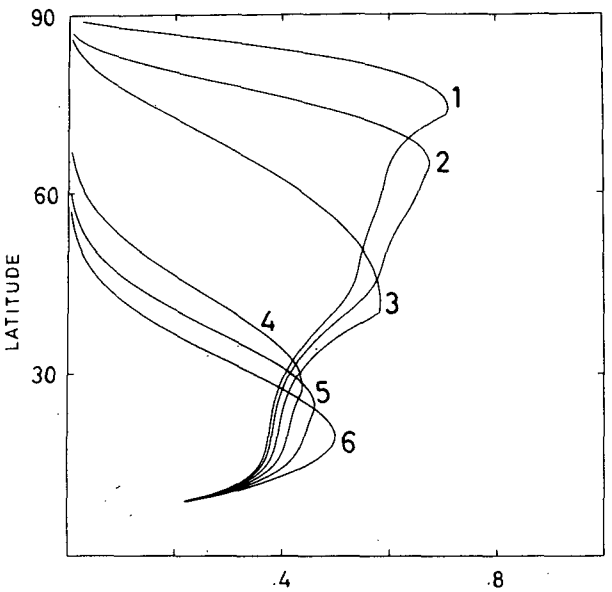

FIG. 14. Amplitudes of the extrema on the rays for different zonal wavenumbers on the 300 mb NH zonal flow.

give a good indication of the extrema exhibited in Fig. 1 for the barotropic model[5] and in Fig. 3 for the baroclinic model. The split in the wavetrains with the long waves going polewards and the shorter waves trapped by the northern flank of the jet is very obvious also for the 30° source shown in Fig. 16a. The worst feature when compared with the simple mountain solution in Fig. 4a of Grose and Hoskins (1979) and Fig. 8 in this paper is the zonal extent of the equatorward wavetrain near latitude 20°. Otherwise, agreement is good. The more poleward source in Fig. 16b gives only long waves propagating polewards and equatorwards in agreement with the 45° source shown in Fig. 4.

Any features which are particularly sensitive to the details of the basic flow are probably not of interest, both because of the variation in the equivalent barotropic level in the baroclinic model solutions and because of lack of validity of the WKBJ solution and, in particular, the criterion (5.22). Thus it is of interest to compare the rays and phases for the 15° source using the 500 mb flow (Fig. 17). The main differences are that wavenumber 4 becomes a long poleward propagating wave and the phase separation and thus apparent wavelengths are somewhat smaller. However, the basic pattern is not sensitive.

In Section 3d it was noted that for 1.2 times the basic winter zonal flow there seemed to be a wavenumber 3 resonance. It is interesting that the zonal wavenumber 3 ray shown in Fig. 16 for the basic 300 mb flow does indicate the possibility of such a wave propagating around a significant portion of the hemisphere. For 1.2 times the basic flow this ray does propagate further around, though this is quite sensitive to the smoothing of the flow. The stationary wavenumber K_s is identical with that which is often referred to as the resonant wavenumber. However, apart from the resonant solution mentioned above, resonance plays no part in the theory and model solutions exhibited here.

Finally, we note that the same wave theories can be applied to a free surface barotropic model. The main change is to replace (5.16) by

$$aK_s = [a^2\beta_M/\bar{u}_M - (a^2\Omega^2/gh)\sin^2 2\phi]^{1/2}. \quad (5.29)$$

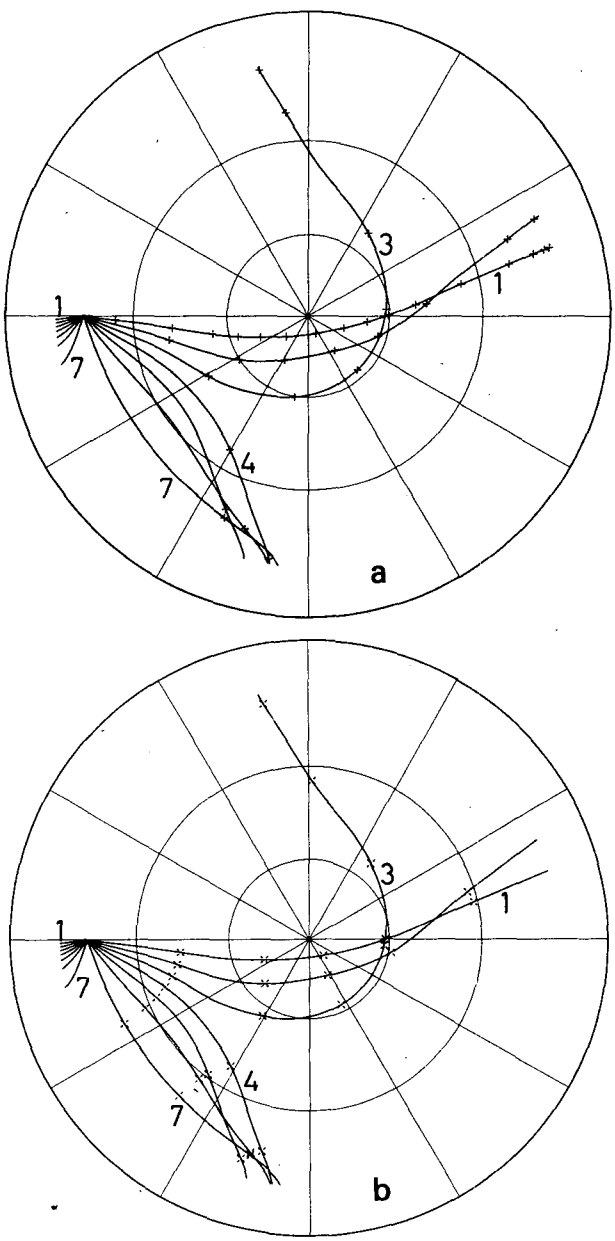

FIG. 15. A 15° source in the NH 300 mb zonal flow: (a) rays and propagation time marked by crosses every 2 days, and (b) rays and phases every 180°.

[5] The barotropic model used a slightly different zonal flow, but neither the rays nor the model solutions are sensitive to this difference.

For an external, barotropic mode we may take an "equivalent depth" $h = 10$ km, so that $a^2\Omega^2/gh \sim 2.2$. Then the stationary wave profiles in Fig. 13, and thus the rays, phases, propagation times and amplitudes are modified by an insignificant amount. This is in agreement with the results of Grose and Hoskins (1979) where it was shown that the simple mountain response was almost identical with an infinite or 10 km depth. However, if one takes $h = 400$ m for the first internal mode, as was done by Gill (1980), then $a^2\Omega^2/gh \sim 55$ and there can be no propagation into middle latitudes. Consistent with the nature of the atmospheric observations and the baroclinic model solutions, this analysis suggests that, away from source regions, the long time-scale middle and high latitude response must have an equivalent barotropic structure.

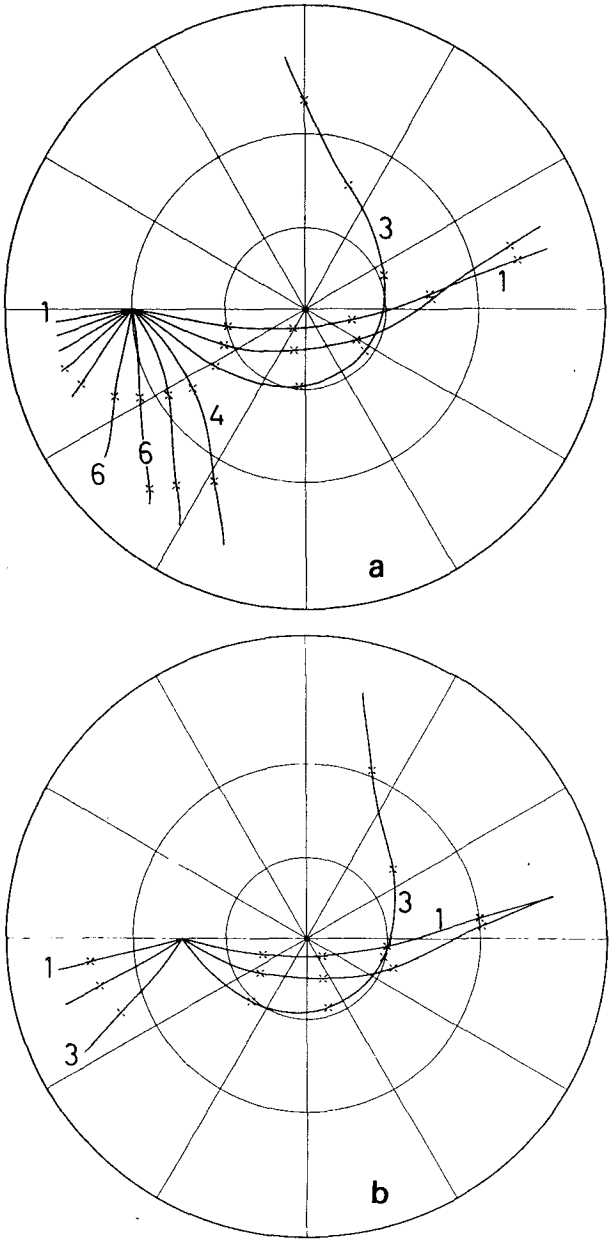

FIG. 16. Rays and phases every 180° for (a) 30° and (b) 45° sources in the NH 300 mb zonal flow.

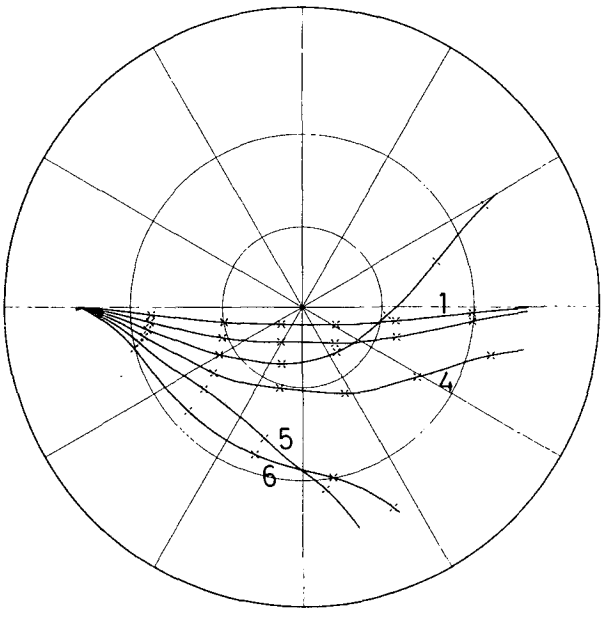

FIG. 17. Rays and phases every 180° for a 15° source in the NH 500 mb zonal flow. Rays for zonal wavenumbers > 6 are omitted.

6. Discussion

In this paper we have concentrated on the patterns generated by forcing in a global atmosphere. Linear barotropic models, baroclinic models and ray tracing analysis have all given similar results which are generally in agreement with those from observational studies and, to some extent, GCM integrations. This gives confidence that the linear, steady-state assumptions do not grossly distort the atmospheric response and that the methods described in this paper provide a good guide to predicting the general pattern of the perturbations induced by large-scale forcing. Whether these methods can predict the positions of the actual extrema is less clear. They should be viewed as part of the hierarchy of models that can be brought to bear on such problems. They suggest modes of behavior that should be looked for in atmospheric and GCM data.

Concurrent with this study, Opsteegh and van den Dool (1980) and Webster (1981), using linear models, have produced results showing the importance for middle latitudes of subtropical forcing in the westerly wind region. This point is clearly in agreement with the work described here.

The role of dissipation in the models used in this paper is an interesting one. If there is very weak dissipation, then resonance is a possibility and the solutions are very insensitive. However, for sufficiently large dissipation, the sensitivity of the

structure of the response disappears. Larger dissipations give the same patterns but with reduced amplitude. The solutions are then much as predicted by frictionless, barotropic ray tracing since the major role of the dissipation is to absorb the waves at the critical line and thus prevent propagation back to the source region. The scale of the response K_s should be interpreted as the local stationary wavenumber and not the resonant wavenumber. This is consistent with the barotropic integrations in which this local scale is established long before Rossby wave energy has had time to propagate around the sphere.

This paper has been concerned with the patterns of the waves induced by large-scale forcing. The fluxes of heat, momentum and potential vorticity by the waves and their Eliassen-Palm fluxes are all subjects of current study, as also is the effect of better resolving the stratosphere.

Acknowledgments. One of us (BJH) gratefully acknowledges the input of Professor J. M. Wallace and others at the Department of Atmospheric Sciences in the University of Washington during an enjoyable summer with them. The paper has also benefited from the comments of Professor R. P. Pearce, Dr. H. C. Davies, Dr. I. Held and Dr. A. J. Simmons. The award of a Shell Australian Postgraduate Scholarship has supported DJK during this study. A portion of this research was carried out at the 1978 NCAR Summer Colloquium and some of the results appeared in the proceedings of that Colloquium. Some of the program development was done in collaboration with the late Dr. N. V. West.

REFERENCES

Bjerknes, J., 1966: A possible response of the atmospheric Hadley circulation to equatorial anomalies of ocean temperature. *Tellus*, **18**, 820–829.

Blackmon, M. L., R. A. Madden, J. M. Wallace and D. S. Gutzler, 1979: Geographical variations in the vertical structure of geopotential height fluctuations. *J. Atmos. Sci.*, **36**, 2450–2466.

Bretherton, F. P., and C. J. R. Garrett, 1969: Wavetrains in inhomogeneous moving media. *Proc. Roy. Soc. London*, **A302**, 529–554.

Charney, J. G., and A. Eliassen, 1949: A numerical method for predicting the perturbations of the middle latitude westerlies. *Tellus*, **1**, 38–54.

Chervin, R. M., J. E. Kutzbach, D. D. Houghton and R. G. Gallimore, 1980: Response of the NCAR general circulation model to prescribed changes in ocean surface temperature. Part II: Midlatitude and subtropical changes. *J. Atmos. Sci.*, **37**, 308–332.

Derome, J., and A. Wiin-Nielsen, 1971: The response of a middle-latitude model atmosphere to forcing by topography and stationary heat sources. *Mon. Wea. Rev.*, **99**, 564–576.

Dingle, R. B., 1973: *Asymptotic Expansions: Their Derivation and Interpretation.* Academic Press, 521 pp.

Egger, J., 1976a: The linear response of a hemispheric two-level primitive equation model to forcing by topography. *Mon. Wea. Rev.*, **104**, 351–364.

——, 1976b: On the theory of steady perturbations in the troposphere. *Tellus*, **28**, 381–389.

——, 1977: On the linear theory of the atmospheric response to sea surface temperature anomalies. *J. Atmos. Sci.*, **34**, 603–614.

Gill, A. E., 1980: Some simple solutions for heat-induced tropical circulations. *Quart. J. Roy. Meteor. Soc.*, **106**, 447–462.

Grose, W. L., and B. J. Hoskins, 1979: On the influence of orography on large-scale atmospheric flow. *J. Atmos. Sci.*, **36**, 223–234.

Held, I., 1978: The vertical scale of an unstable baroclinic wave and its importance for eddy heat flux parameterizations. *J. Atmos. Sci.*, **35**, 572–576.

Horel, J. D., and J. M. Wallace, 1981: Planetary-scale atmospheric phenomena associated with the Southern Oscillation *Mon. Wea. Rev.*, **109**, 813–829.

Hoskins, B. J., 1980: Representation of the earth topography using spherical harmonics. *Mon. Wea. Rev.*, **108**, 111–115.

——, and A. J. Simmons, 1975: A multi-layer spectral model and the semi-implicit method. *Quart. J. Roy. Meteor. Soc.*, **101**, 637–655.

——, A. J. Simmons and D. G. Andrews, 1977: Energy dispersion in a barotropic atmosphere. *Quart. J. Roy. Meteor. Soc.*, **103**, 553–567.

Lau, N. C., 1979: The observed structure of tropospheric stationary waves and the local balances of vorticity and heat. *J. Atmos. Sci.*, **36**, 996–1016.

Lighthill, J., 1978: *Waves in Fluids.* Cambridge University Press, 504 pp.

Longuet-Higgins, M. S., 1964: Planetary waves on a rotating sphere, I. *Proc. Roy. Soc. London*, **A279**, 446–473.

Kasahara, A., T. Sasamori and W. M. Washington, 1973: Simulation experiments with a 12-layer stratospheric global circulation model, I: Dynamical effect of the earth's orography and thermal influence of continentality. *J. Atmos. Sci.*, **30**, 1229–1251.

Manabe, S., and T. B. Terpstra, 1974: The effects of mountains on the general circulation of the atmosphere as identified by numerical experiments. *J. Atmos. Sci.*, **31**, 3–42.

Opsteegh, J. D., and H. M. van den Dool, 1980: Seasonal differences in the stationary response of a linearized primitive equation model: Prospects for long range weather forecasting? *J. Atmos. Sci.*, **37**, 2169–2185.

Phillips, N. A., 1973: Principles of large-scale numerical weather prediction. *Dynamical Meteorology*, P. Morel, Ed., Reidel, 1–96.

Rowntree, P. R., 1972: The influence of tropical east Pacific Ocean temperatures on the atmosphere. *Quart. J. Roy. Meteor. Soc.*, **98**, 290–321.

——, 1976a: Tropical forcing of atmospheric motions in a numerical model. *Quart. J. Roy. Meteor. Soc.*, **102**, 583–606.

——, 1976b: Response of the atmosphere to a tropical Atlantic ocean temperature anomaly. *Quart. J. Roy. Meteor. Soc.*, **102**, 607–626.

Smagorinsky, J., 1953: The dynamical influence of large-scale heat sources and sinks on the quasi-stationary mean motions of the atmosphere. *Quart. J. Roy. Meteor. Soc.*, **79**, 342–366.

Tung, K. K., 1979: A theory of stationary long waves, Part III: Quasi-normal modes in a singular waveguide. *Mon. Wea. Rev.*, **107**, 751–774.

Wallace, J. M., and D. S. Gutzler, 1981: Teleconnections in the geopotential height field during the Northern Hemisphere winter. *Mon. Wea. Rev.* **109**, 784–812.

Webster, P. J., 1981: Mechanisms determining the atmospheric response to sea surface temperature anomalies. *J. Atmos. Sci.*, **38**, 554–571.

Whitham, G. B., 1960: A note on group velocity. *J. Fluid Mech.*, **9**, 347–352.